Threshold effect on whole-cell catalysis of extra hyperviscous biosystem by a sealed oxygen supply biotechnology

Yong XU[1], Xia Hua[1], YaTing Hu[1], Jian Han[1], HongSheng Zhang[1], and Xin Zhou[1]

[1]Nanjing Forestry University

March 15, 2024

Abstract

The end-product concentration and productivity are critical issues in economic competition between biotechnological commercials and the chemical engineering industry. The prominent contradiction between high-titer products and the large-scale oxygen demand for aerobic biocatalysis leads to hyperviscosity, mass transport bottleneck in [dynamically changing](javascript:;) polyphase biosystems, and severe foaming problems. In this study, an intensification strategy for the whole-cell catalytic preparation of high-titer xylonic acid by *Gluconobacter oxydans* in a sealed-compressed oxygen supply bioreactor is propose. Multi-scale control factors are quantitatively studied to determine the biochemical parameter thresholds, and theoretically calculated the optimal production performance based on threshold effect. Finally, 650.8 g/L xylonic acid is obtained with a maximum productivity of 41.7 g/L/h with a catalytic performance of 95.8%, compared with the theoretical calculations. The intensification strategy for the oxygen transfer threshold effect overcome the stubborn obstacles of obligate aerobic catalysis, while providing a sustainable value-added pathway for fermentative lignocellulose.

Hosted file

`Figure.docx` available at https://authorea.com/users/502489/articles/726613-threshold-effect-on-whole-cell-catalysis-of-extra-hyperviscous-biosystem-by-a-sealed-oxygen-supply-biotechnology

Hosted file

`Table.docx` available at https://authorea.com/users/502489/articles/726613-threshold-effect-on-whole-cell-catalysis-of-extra-hyperviscous-biosystem-by-a-sealed-oxygen-supply-biotechnology

Threshold effect on whole-cell catalysis of extra hyperviscous biosystem by a sealed oxygen supply biotechnology

Xia Hua[a, b, c], YaTing Hu[a, b, c], Jian Han[a, b, c], HongSheng Zhang[a, b, c], Xin Zhou[a, b, c], Yong Xu[a, b, c *]

[a] *Key Laboratory of Forestry Genetics & Biotechnology (Nanjing Forestry University), Ministry of Education, Nanjing 210037, People's Republic of China*

[b] *Jiangsu Co-Innovation Center of Efficient Processing and Utilization of Forest Resources, College of Chemical Engineering, Nanjing Forestry University, Nanjing 210037, People's Republic of China*

[c] *Jiangsu Province Key Laboratory of Green Biomass-based Fuels and Chemicals, Nanjing 210037, People's Republic of China*

***** Corresponding author at: College of Chemical Engineering, Nanjing Forestry University. No. 159 Longpan Road, Nanjing 210037. People's Republic of China.

E-mail address: xuyong@njfu.edu.cn (Y. X.)

Tel: +86 025 85427587

Fax: +86 025 85427587

Abstract

The end-product concentration and productivity are critical issues in economic competition between biotechnological commercials and the chemical engineering industry. The prominent contradiction between high-titer products and the large-scale oxygen demand for aerobic biocatalysis leads to hyperviscosity, mass transport bottleneck in dynamically changing polyphase biosystems, and severe foaming problems. In this study, an intensification strategy for the whole-cell catalytic preparation of high-titer xylonic acid by *Gluconobacter oxydans* in a sealed-compressed oxygen supply bioreactor is propose. Multi-scale control factors are quantitatively studied to determine the biochemical parameter thresholds, and theoretically calculated the optimal production performance based on threshold effect. Finally, 650.8 g/L xylonic acid is obtained with a maximum productivity of 41.7 g/L/h with a catalytic performance of 95.8%, compared with the theoretical calculations. The intensification strategy for the oxygen transfer threshold effect overcome the stubborn obstacles of obligate aerobic catalysis, while providing a sustainable value-added pathway for fermentative lignocellulose.

Keywords: Whole-cell catalysis; Threshold effect; Oxygen transfer; Process intensification strategy; Computational fluid dynamics.

Introduction

Modern industrial microbial fermentation/catalysis processes are mainly performed by (obligate) aerobic microorganisms, such as amino acid produced by *Corynebacterium*, organic acid from *Aspergillus niger*, and many antibiotic fermentations are aerobic fermentation[1-3]; three products are platform compounds with the largest global market share. These aerobic microorganisms consume molecular oxygen as a final electron acceptor in the electron transport chain, determining the strong oxygen dependence of bioprocess[4,5]. At normal temperature and pressure, the oxygen saturation solubility in broth is approximately 0.2 mmol/L, equivalent to a stoichiometric 6.4 mg/L[6]. However, taking common metabolic substrate glucose as an example, the respiratory metabolism process can be expressed as $C_6H_{12}O_6+6O_2 \rightarrow 6H_2O+6CO_2+$energy, indicating that 6 mol (192 g) of oxygen is required to oxidize 1 mol (180 g) of glucose[7]. For an incomplete oxidation, 1 mol (180 g) of glucose oxidation consumes around 0.5 mol (16 g) of oxygen[8]. Notably, compared with the glucose saturation solubility(70% *W/V*), the oxygen saturation solubility is approximately 18,000~20,000 times lower[9]. Hence, this large difference in solubility between solute and oxygen results in the normal physiological activity of microorganisms in fermented broth maintained for 15~20 seconds without a continuous gas supply. Additionally, with the continuous improvement in production levels, such as the strains' directional evolution and the equipment upgrading, the oxygen supply capacity in industrial production has become stringent[10,11]. Therefore, the relationship between oxygen supply and

demand in the bioprocess is crucial in exploring and optimizing the biocatalysis conditions.

In aerobic fermentation/catalysis, the oxygen supply of microorganisms involves the gas phase oxygen, which is first dissolved in the broth to form dissolved oxygen (DO), then transmitted to cell membrane dehydrogenase or intracellular respiratory enzyme site for oxidation/respiration[12]. The transfer process can be further divided into oxygen supply and consumption, as shown in Figure 1. Oxygen supply refers to the oxygen from the air bubble through the gas phase, gas film, and gas-liquid interface and finally diffusion into the liquid phase. Oxygen consumption refers to the oxygen molecules diffusion process into the cell from the liquid phase via liquid membrane, liquid-solid interface, and cell membrane. Therefore, oxygen must overcome nine mass transfer resistances shown in Figure 1 during transport to reach the reaction site before microorganisms can use it, suggesting the impact of intensified oxygen transport during aerobic fermentation/catalysis[13,14].

Theoretical mass intensification during the oxygen transport process is conducted in two aspects: oxygen transfer rate (OTR) and oxygen uptake rate (OUR)[15-17]. According to the two-film theory model, equation (1) describes the oxygen transport efficiency between multiphases during the oxygen supply stage[18].

$$(1)\ OTR = K_L\alpha \cdot (C^* - C_L)$$

Where K_L is the oxygen mass transfer coefficient (m/h), α indicates the specific surface area of the liquid film (m^2/m^3), and C^*/C_L describes the saturated/actual DO concentration (mmol/L). In industry, K_L and α are usually combined into one index,

the volume transfer coefficient $K_L\alpha$, a significant parameter to simulate the aerobic microorganisms bioprocess' and reactor scale-up[19]. The relationship between α and gas holdup (α_g) with fluid/gas volume is given in equations (2) and (3)[20].

$$(2)\ \alpha = \frac{A_s}{v_L + v_G}$$

$$(3)\ \alpha_g = \frac{v_G}{v_L + v_G}$$

Where A_s is the total liquid film area (m^2) and V_L/V_G is the liquid/gas volume in a bioreactor (m^3).

Substituting equation (3) into equation (2) describes the relationship between α and α_g, as shown in equation (4).

$$(4)\ \alpha = \frac{6}{d_B} a_g$$

Where d_B is the bubble diameter.

Since saturated DO concentration C* is relatively stable under specific fermentation/catalytic conditions, the main perspective of OTR intensification is to improve the gas holdup α_g in bioprocesses (Equation 4). Moreover, the oxygen consumption rate during aerobic cell reactions determines the OTR from the gas to the liquid phase, and OUR is calculated by equation 5[21].

$$(5)\ OUR = q_{O_2} \cdot C_x$$

Where q_{O_2} is the specific rate of oxygen consumption ($mol/(m^3 \cdot s)$) and C_x shows the cell concentration.

When the inoculation amount is fixed, the cell respiration rate determines the OUR intensity. Therefore, from the two-stage oxygen transport theory, developing a novel intensification strategy for $K_L\alpha/\alpha_g/q_{O_2}$ can provide a promising approach to

solve the inherent bottlenecks in traditional aerobic biocatalysis, especially in highly viscous reaction systems.

Herein, a typical specific aerobic gram-negative bacteria, *Gluconobacter oxydans* (*G. oxydans*), is a biocatalyst to emphasize power consumption and oxygen transfer evaluation for C5 sugar acid production for practical applications[22,23]. *G. oxydans* is a common industrial microorganism in industry due to its incomplete oxidation and several membrane-bound dehydrogenases, generating a wide range of products, such as ascorbic acid, sugar acid, glycolic acid, 1,3-dihydroxyacetone, and other value-added compounds[24-26]. The fluid rheological characteristics and related parameters are first evaluated for a high-viscosity reaction system in preparing high-titer xylonic acid (XA) by whole-cell catalysis of *G. oxydans*. The relationship between rotation speed and gas holdup α_g, stirring power, respiration rate q_{O_2} and volume transfer coefficient $K_L\alpha$ is explored, and various parameters' threshold is quantitatively determined based on the fluids' rheological characteristics, combined with computational fluid dynamics (CFD) and dynamic mechanism of oxygen supply/consumption analysis[27,28]. Finally, a specific process intensification strategy is established from the threshold effect, and challenges associated with oxygen in the gas-liquid and liquid-solid transport process in the high-viscosity reaction system are simultaneously solved, achieving a breakthrough improvement in producing xylonic acid from sustainable lignocellulose raw materials.

Materials and Methods

Microorganism and chemicals

Microorganism: The biocatalyst used in this study was *G. oxydans* NL71, obtained from *G. oxydans* ATCC 621, usually stored in sorbitol-agar medium at 4°C. The strain activation and proliferation process were continuously cultured for 24-36 h in sorbitol (50 g/L) and yeast extract medium (5 g/L) at 30°C and 220 rpm[29].

Chemicals: All chemicals and reagents are commercially available analytical grade for the experiments. Additionally, sorbitol, xylose, and nutrient salts were purchased from Sinopharm Co., LTD; XA and yeast extracts were obtained from Sigma-Aldrich Co., LTD.

The whole-cell catalysis

Bioreactor model: This study was conducted in a 5 L sealed oxygen supplied bioreactor (SOS-BR) (BIOTECH-5JG, BXBIO, China), composed of double-layer stirring paddles and four baffles of 10 mm width, uniformly provided inside the tank wall, meeting the "full baffle condition". The paddle type was a six-straight blade paddle with a distance of 70 mm between two paddles. Air/oxygen was introduced to the bioreactor through an air ring-shaped sparger 3 mm from the bottom, containing 17 equally spaced upward holes (1 mm diameter). Considering the bioreactor model complexity and high requirements for grid quality for CFD simulations, the specific bioreactor parameters were selected, as shown in Table 1[27].

Biocatalysis process: The whole cell catalysis was performed in SOS-BR with 99.9% pure oxygen through pressure sensors to achieve automatic and continuous pressure stabilization. This oxygen supply method achieved maximum oxygen utilization and realized most economical production, performed at 500 rpm and

30 ℃ with 3 L broth containing *G. oxydans* (10 g/L), xylose (100-800 g/L), yeast extract (10 g/L), $MgSO_4$ (0.5 g/L), KH_2PO_4 (1 g/L), K_2HPO_4 (2 g/L) and $(NH_4)_2SO_4$ (2 g/L)[30]. The internal pressure of the bioreactor was maintained at 0.05 mPa, and the pH was adjusted at 5.5 by 30% NaOH.

Determination of viscosity and density

Viscosity: The viscosity of xylose and XA reaction systems at different concentrations was measured by portable viscosity electrodes (XL7-100B-d15) purchased from Hemmerson Co., LTD., UK.

Density: The density at different concentrations was measured by the mass volume method.

CFD simulation

Meshing: Non-structural meshing of bioreactor models was performed by pre-processing Fluent Meshing software. During the simulation of the bioreactor's internal flow field, the stirring shaft's influence on the numerical simulation results was minimal; therefore, the stirring shaft was simplified. The meshes at paddles, holes, and interfaces were also increased to improve the accuracy of the calculation. After adaptive meshing, the total number of meshes and nodes was 1,992,903 and 370,268, and all underwent non-dependency testing. The schematic meshing of the bioreactor is shown in Figure 2.

Calculation condition: Since the gas-liquid phases in the bioreactor exhibited their motion characteristics, a widely-used Euler-Euler multiphase model was employed, and continuity and phase momentum equations such as equations 6 and 7

were used[31,32].

$$(6)\ \frac{\partial}{\partial t}(\rho_i \alpha_i) + \nabla \cdot (\alpha_i \rho_i \overrightarrow{v_i}) = 0$$

Where α_i, ρ_i, $\overrightarrow{v_i}$ are the density, volume fraction, and average velocity of each phase.

$$(7)\ \frac{\partial}{\partial_t}(\alpha_i \rho_i \overrightarrow{v_i}) + \nabla \cdot (\alpha_i p_i \overrightarrow{v_i} \cdot \overrightarrow{v_i}) = -\alpha_i \nabla p + \nabla \cdot \overline{\overline{\tau_i}} + \overrightarrow{R_i} + \alpha_i \rho_i \vec{g}$$

Where $\overrightarrow{R_i}$ is the interaction force between phases, p indicates the pressure shared by two phases, $\vec{g}$ shows acceleration due to gravity and $\overline{\overline{\tau_i}}$ is the pressure-strain tensor.

The dynamic and static region processing method adopted the multiple reference frame (MRF) method, and the *k-ε* turbulence model was selected to solve the unsteady state. Since the sensitivity of the study to bubble size was weak, the bubble diameter was uniformly set to 4 mm according to theoretical experience. The broth viscosity and density were adjusted accordingly, and the oxygen viscosity and density were set to 1.789×10^{-5} kg·m^{-1}·s^{-1}, and 1.429 kg·m^{-3}, respectively. The simulated working condition was 1 L/min ventilation, equivalent to the ventilation line speed of 1.25 m/s per air dispersion hole, and the rotation speed was set at 100 rpm-1000 rpm. α_g and the moment coefficient of the stirring shaft were monitored, and calculations were stopped when the parameters reached a steady state.

Boundary conditions: 1) Set the fluid region as the relative stationary region in the bioreactor, the propeller as the rotation region, and the interface between two regions as a boundary. 2) Set tanks, baffles, and air dispersers as stationary wall boundary conditions. 3) The gas inlet boundary was set to a uniform velocity inlet

boundary condition, and the gas volume fraction was set to 1. 4) The top of the bioreactor was set as the pressure outlet boundary, and the outlet boundary conditions were maintained to conserve the mass (overall gas and liquid). 5) Considering gravity's influence, set gravity's acceleration to 9.81 m/s^2.

α_g and P calculation: α_g was obtained from the CFD simulation. The stirring power and power number were calculated by and equations 8 and 9.

(8) $P = 2\pi NM$

(9) $N_P = P \,/\, \left(pN^3D^5\right)$

Where P denotes power (W), N depicts rotation speed (r·s^{-1}), M illustrates torque provided by CFD simulation (N·m), Np is power number, ρ shows broth density (kg·m^{-3}), and D is paddle blades diameter (m).

Dynamic measurement process of oxygen transfer

Calibration: In the DO level calibration process, define the oxygen concentration in 5% sodium sulfite solution as 0% DO level, and the oxygen concentration in water at 500 rpm and 3 L/min as 100% DO level.

Dynamic method: The oxygen transport parameters were calculated by the dynamic determination process, divided into three stages[33]. The first stage was the stable gas supply, where the DO level remained stable. The second stage was the stop gas supply, where the DO level in the broth quickly decreased due to *G. oxydans* consumption. The gas supply was restored when the DO level dropped in the second stage.; In the third stage, the DO level returned to a high point and gradually stabilized. The dynamic change curve in DO was recorded online using a

DO electrode. Figure 3 shows the variation in DO level for the dynamic method.

q_{O_2} and $K_L\alpha$ calculation: The equation for q_{O_2} was mainly based on the second stage free oxygen consumption rate, calculated from equation 10.

$$(10)\ \frac{\mathrm{d}c}{\mathrm{d}_t} = -\ q_{O_2} C_x$$

The accounting equation for $K_L\alpha$ was mainly based on the change in DO level when the air supply was restored in the third stage, calculated as equation 11.

$$(11)\ \ln\left[\frac{C_L^{t=\infty} - C_L^{t=t_1}}{C_L^{t=\infty} - C_L^{t=t_2}}\right] = k_L\alpha(t_2 - t_1)$$

where, $C_L^{t=t_1}$ $C_L^{t=t_2}$ and $C_L^{t=\infty}$ represent DO values at different time points.

Analytical methods

The xylose and XA concentrations were quantified by high-performance anion-exchange chromatography (HPAEC) equipped with a pulsed amperometric detector (Thermo ICS-5000). Detection conditions were as follows: The chromatographic column was CarboPac™ PA10, the mobile phase was 100 mM NaOH, the flow rate was 0.3 mL/min, and the detection time was 30 min[34].

Three parallel assays were performed for each experiment.

Results and discussion

Determination of xylose/XA fermentation broth physical parameters

Density and viscosity are internal friction metrics in fluids and affect their physical properties[35]. Most non-Newtonian fluids in food and construction industries are pseudo-plastic fluids, especially polymer solutions, and suspensions with shear-thinning characteristics[36]. Therefore, exploring the physical parameters of fluids has theoretical significance in strengthening their mass transfer capacity.

Therefore, the viscosity and density of xylose/XA fermentation broth in the 0-800 g/L concentrations are measured (Figure 4). The density variation trend with concentration is shown in Figure 4A, indicating a direct proportional relationship. The relationship between xylose concentration and density is $y=3.60\times10^{-4}x+0.999$, $R^2=0.998$, while that of XA concentration and density is $y=3.66\times10^{-4}x+1.007$, $R^2=0.998$. Figure 4B shows the changes in xylose and XA viscosity at different concentrations. Nonlinear curve fitting of viscosity at different concentrations shows an exponential relationship between two parameters, indicating that the correlation between xylose for and XA concentration and viscosity is $y=1.0e^{0.0033x}-0.14$, $R^2=0.998$ and $y=0.7e^{0.0037x}+0.22$, $R^2=0.997$, respectively. Moreover, the viscosity of the same concentration of xylose fermentation broth is greater than that of XA fermentation broth, suggesting that the viscosity theoretically decreased gradually due to the incomplete xylose oxidation to XA during the whole cell catalysis. Since the main goal is to intensify the mass transfer capacity in hypertonic/hyperviscous systems, subsequent rheological parameter calculations and CFD simulations are based on viscosity at initial xylose concentration.

Rheological characterization of xylose/XA at different system conditions

Rheological properties of fermented broth are closely related to physical, chemical, and biological parameters of bioprocess based on process modeling and controlling optimization of the "reactor ecosystem", and changes in these properties directly affect the mixing state and mass/heat transfer rate of fermentation broth[37]. For non-Newtonian fluids with independent rheological properties of shear time, the

relationship between shear force τ and shear rate γ is expressed by the power law $\tau=k\gamma^n$. The flow characteristic index n and consistency coefficient k jointly determine the flow behavior. Therefore, determining these two rheological parameters by flow characteristic equation can solve the non-Newtonian liquid transport calculation. To theoretically calculate flow characteristic parameters, the first logarithm is taken based on the traditional non-Newtonian fluid flow characteristic formula (equation 12) to obtain equation 13[38].

$$(12)\ \eta = k \cdot \gamma^{n-1}$$

$$(13)\ ln\,\eta = ln\,k + ln\,\gamma^{n-1}$$

Where η represents broth viscosity (mPa·s), k indicates consistency coefficient ($N \cdot s^n/m^2$), n depicts characteristic index (the degree of liquid deviation from a Newtonian fluid), and γ denotes shear rate (s^{-1}).

Moreover, transforming equation 13 yielded equation 14.

$$(14)\ ln\,\eta = ln\,k + (n-1)\,ln\,\gamma$$

The relationship between shear rate and speed was equation 15 for stirred bioreactors[31].

$$(15)\ \gamma = K_{(N)} \cdot N_i$$

Where $K_{(N)}$ represents the stirring constant, and N_i is the stirring speed (rpm).

By introducing equation 14 to equation 15 and modifying it to obtain equation 16, the mathematical model is proposed to calculate the rheological properties parameters.

$$(16)\ ln\,\eta = ln\,(k \cdot K^{n-1}) + (n-1)\,ln\,N_i$$

From equation 16, the relationship between η and N_i conforms to a linear equation using a two-log system, with a slope of $(n-1)$ and an intercept of $ln(k \cdot K^{n-1})$. Therefore, the rheological parameters are calculated by determining the viscosity of broth at different concentrations and stirring speeds.

To quantify the rheological properties of the reaction system, the viscosity of the broth is measured at different stirring speeds. Figure 5A-F shows viscosity trends of the xylose system at 50-500 g/L concentration. Results reveal that the viscosity change law describes a two-stage trend. In the first stage, the viscosity decreases exponentially when the speed is lower than 600 rpm. In the second stage, when the speed was higher than 600 rpm, the viscosity increased linearly, and a specific mathematical relationship is drawn. Theoretically, for pseudoplastic fluids in non-Newtonian fluids, the viscosity of a liquid decreases with the increase in stirring degree and shows obvious shear thinning characteristics, contradicting the results in Figure 5. Obviously, the viscosity change trend at a rotation speed of less than 600 rpm follows the fluid characteristic law. In contrast, the viscosity change trend is abnormal at a rotation speed higher than 600 rpm since the broth forms countless small bubbles under high-speed stirring conditions of the large bioreactor stirring paddle (D=88mm), substantially increasing the internal friction between fluid molecules, thereby, linearly increasing the broth viscosity.

Additionally, when the xylose concentration in broth increases to 600-800 g/L, the relationship between viscosity and rotation speed is illustrated in Figure 5G-I. Obtained results reveal that the change in viscosity under the

hypertonic/hyperviscous system is similar to that of a low-concentration reaction system with a different turning point of viscosity change. The viscosity of the low-viscosity system rebounds when the rotation speed is higher than 600 rpm, while the hypertonic/hyperviscous system is 700 rpm since the high viscosity hinders the bubbles formation, and only at higher rotational speeds can intensify the internal friction, thus, linearly increasing the viscosity. As is well known, the lower the broth viscosity, the more favorable the whole-cell catalytic effect. Therefore, based on mass transfer intensity and lower viscosity, the first threshold range for rotation speed under different xylose concentrations is determined as 400-650 rpm for 50-500 g/L and 400-750 rpm for 600-800 g/L (Figure 5).

Considering the shear-thinning characteristics of the quasi-plastic fluid, subsequent calculations of the fluid characteristic index are based on viscosity change in the first stage. According to equation 16, the viscosity and rotation speed are logarithmically fitted (Figure 5), and results are shown in Figure 6a, indicating a good linear relationship between Inη and InN at different xylose concentrations. The specific linear fitting formulas are shown in Figure 6.

Since the stirring paddle diameter to bioreactor diameter ratio is 88 mm: 170 mm=0.52≈0.5, the stirring constant K is taken as 2.4. Finally, the flow characteristic index n and consistency coefficient k are calculated from the slope and intercept of the fitted formula (Table 2). The results reveal that the flow characteristic index n decreases with the increase in xylose concentration, indicating that a greater broth viscosity leads to greater liquid deviation from the Newtonian fluid. Moreover, the

consistency coefficient k increases with the increase in xylose concentration, indicating an obvious viscosity-limiting effect of broth. Apparently, the change law of rheological parameters confirms the strong resistance of hypertonic/hyperviscous systems to mass transfer. Finally, this study established a mathematical calculation model for the fluid characteristic parameters of hypertonic/hyperviscous xylose fermentation broth by combining experiments and mathematical formulas, providing solid theoretical and data support for subsequent CFD simulation and oxygen transport mechanism analysis.

CFD simulation for the influence of rotation speed on flow field characteristics

With continuous development in computer technology and numerical simulation calculation methods, CFD is widely used in modern science and engineering research as an emerging discipline[39]. Combined with fluid dynamics theory, numerical calculation methods, and data visualization technology, CFD can simulate and analyze physical phenomena, including flow properties, heat transfer, and mechanical motion in a flow field[40]. Therefore, CFD has become a powerful tool to overcome the flow and mass transfer challenges in the flow field. Rotation speed is an important parameter affecting the fluid velocity, gas residence time, and gas-liquid mixing time in a bioreactor; therefore, CFD is employed to simulate the internal flow field, and the influence of rotation speed on power characteristics and local gas content is compared.

Gas holdup α_g is the gas phase volume fraction in the reactor, the main index to evaluate the gas dispersion performance of the bioreactor[41]. Moreover, it is also

important in bioreactor amplification design, affecting other hydrodynamic parameters such as flow pattern and gas-liquid contact area. The cloud diagram of gas distribution in the middle cross-section of a bioreactor with xylose different concentrations (100/300/500/700 g/L) and rotation speeds (100/300/500/700/900 rpm) are illustrated in Figure 7. Results show that in the same xylose concentration system, the stronger the degree of agitation leads to a greater radial velocity, and the gas is rapidly pushed toward the tank wall, making the gas distribution more widespread and uniform. Additionally, under the same rotation speed, the gas distribution in the broth did not change significantly, indicating that certain stirring intensities could overcome the mass transfer limiting effect of broth viscosity on the gas.

In order to compare the effect of rotation speed on mass transfer more intuitively, the average gas holdup α_g is further analyzed (Figure 8a). The results reveal that the change law of gas holdup α_g is similar to the gas distribution and the gas holdup α_g is positively correlated with stirring strength and negatively correlated with viscosity. Obviously, the stirring strength significantly improves the gas holdup α_g in the bioreactor. Moreover, the prerequisite to increase the DO level is a sufficient supply of gas components, and the oxygen driving force is polished after the increase in DO level, ultimately achieving the goal of strengthening OTR. Therefore, 10% gas holdup αg is the lowest reasonable limit to establish the optimal mass transfer intensification strategy. Based on this value, the second threshold is determined for the rotation speed of the reaction system with different xylose

concentrations. The threshold range is shown in Figure 8c.

In the gas-liquid two-phase simulation of fermentation/catalysis, power number is an important parameter representing power consumption during paddle stirring[42]. When the blade type is kept constant during the simulation, the smaller power number will consume less power. Therefore, studying the power number positively impacts the stirring efficiency. Based on CFD technology, the corresponding torque is obtained by simulating fluid processes under different conditions, and the power number is calculated by equations (8) and (9), as shown in Figure 8b. The results demonstrate that the power number positively correlates with xylose concentration and negatively correlates with the rotational speed. To improve economic competitiveness as a requirement, when the xylose/XA concentration gradually accumulates in the whole-cell catalysis, increasing the rotation speed is necessary to control the power number at a low level. Therefore, 2.5 of the power number is set as a judging value, and the third threshold is determined from the rotation speed with different xylose concentrations (Figure 8c). CFD is employed to simulate the fluid flow field under different conditions, investigating the gas distribution, gas holdup, power number, and other related parameters and determining the rotation speed threshold range, providing reference indicators to establish an economically competitive mass transfer intensification strategy.

Influence of rotation speed on oxygen transfer parameters

Previous CFD simulation-based studies have reported the specific conditions of high oxygen margin in different reaction systems, providing an oxygen-rich

environment to analyze the dynamic mechanism of oxygen supply/consumption in whole-cell catalysis by *G. oxydans*. The oxygen transfer parameters are further determined by the dynamic method. The dynamic measurement process quantitatively investigates the DO level to calculate the cell respiration rate. q_{O_2} and volume transfer coefficient $K_L\alpha$ (equations (10) and (11)). Taking the rotation speed condition of 500 rpm as an example, the change in DO levelduring the dynamic evaluation of oxygen transfer parameters under different xylose concentrations is shown in Figure 3. Wherein, Figure 9a shows the variations in DO level at 100 rpm to 500 rpm rotation speed, indicating that the stable DO level during the first stage increases with the rotation speed. Moreover, the rate of change in DO level during the second stage oxygen consumption process and third stage oxygen supply process significantly improved with the increase in rotation speed. However, when the rotation speed exceeds 500 rpm, there as a qualitative difference between the variation pattern of DO level (Figure 9b). Obviously, when the string intensity is large enough, the DO level in the broth reaches saturation and does not increase with rotation speed. The main difference is that in the second stage, when the oxygen supply to the bioreactor is stopped, the rate of free oxygen consumption by microorganisms negatively correlates with the rotation speed, theoretically representing the limited respiratory capacity of *G. oxydans*. During the third stage, the DO levels show a rapid rebound trend due to the strong stirring environment, and all recovered to saturation levels in a short period of time.

Specific values of oxygen transfer parameters are further calculated to visually

analyze the impact of rotation speed on oxygen transfer parameters, based on DO level data of the second and third stages according to equations (10) and (11), as shown in Figure 9c. Results reveal that the cell respiration rate q_{O_2} first rise and then decrease with the increase in rotation speed and is the maximum at 600 rpm condition, 2.97 mmol $O_2/g_x/h$. Conversely, the volume transfer coefficient $K_L\alpha$ always maintains an upward trend, and the increasing amplitude is obvious with the increase in stirring intensity. Theoretically, a larger oxygen transfer coefficient results in a better mass transfer effect, suggesting a faster metabolic rate of aerobic microorganisms. However, experimental results indicate a contradiction between the change law of q_{O_2} and $K_L\alpha$, since excessive stirring intensity wastes power and damages the bacteria, leading to autolysis and reduced bacterial production. Therefore, the cell respiration rate q_{O_2} is the main indicator in evaluating the whole-cell catalytic efficiency rather than the oxygen transfer coefficient $K_L\alpha$. At the same time, due to the inability of *G. oxydans* to metabolize xylose, the only oxygen consumption pathway in the second stage is incomplete xylose oxidation to form XA. The stoichiometric ratio between generated XA and consumed oxygen is 2:1 after conversion. Therefore, the maximum theoretical productivity of XA in the xylose (500 g/L) reaction system is about 8.91 g/L/h.

Finally, the relationship between maximum theoretical XA productivity and rotation speed at different xylose concentrations is fitted (Figure 9d), illustrating that the theoretical XA productivity increases first and then decreases. Therefore, controlling the rotation speed within a reasonable range can ensure a higher catalytic

efficiency. Moreover, these results also indicate that the maximum theoretical productivity decreased with the increase in broth viscosity, especially when the xylose concentration exceeds 500 g/L. The large mass transfer resistance reduces XA productivity to less than 10 g/L/h. Therefore, to establish a comprehensive process intensification strategy to maximize the catalytic efficiency of hypertonic/hyperviscous systems, a fourth threshold of rotation speed under different xylose concentrations is further determined in the range of 98% of maximum theoretical productivity (Figure 9e). Overall, the threshold range increases gradually since a more viscous broth leads smaller shear force generated at the same rotation speed, resulting in a higher rotation speed that cells could tolerate. In this study, the variation in oxygen transfer parameters under different conditions is quantitatively investigated. The optimal threshold range is determined, providing an important theoretical basis for breaking through the mass transfer limitation effect of hypertonic/hyperviscous systems.

Whole-cell catalysis based on optimal process intensification strategy

Through fluid characteristic analysis, CFD simulation, and oxygen transfer mechanism exploration, the reasonable rotation speed threshold range is quantified by the change law of broth viscosity, gas holdup, power number, cell respiration rate, and oxygen transfer coefficient, and the parameter threshold range is summarized in Figure 10a. Moreover, the optimal rotation speed at 100 g/L-800 g/L xylose concentration is further determined with the performance of cell respiration rate as a main reference index, 532, 574, 594, 610, 626, 642, 657, and 673 rpm, respectively.

The optimal rotation speed from the threshold effect is non-linearly fitted to obtain the theoretical mathematical model of optimal rotation speed in whole-cell catalysis, providing a technical basis for an aerobic biocatalytic synthesis of XA by *G. oxydans* (Figure 10b). Additionally, the Figure 10b also lists the maximum theoretical XA productivity at various xylose concentrations, and the data shows a significant decrease in catalytic efficiency in hypertonic/hyperviscous systems, indicating the necessity and urgency of overcoming mass transfer restriction effects in the aerobic catalytic industry.

In whole-cell catalysis, there are stubborn substrate, product inhibition, and mass transfer obstruction. To maximize the titer of the final product in a single batch, the product inhibition effect is inevitable; however, the substrate inhibition effect is usually effectively overcome through a batch-feeding mode. Therefore, integrating the maximum theoretical productivity at different xylose concentrations (Figure 10b) can realize the optimal catalytic process (red line in Figure 10c). According to the integration results illustrate the theoretical maximum XA titer within 48 h is 679.3 g/L, maximum productivity is 44.4 g/L/h, and average productivity is 14.2 g/L/h. Furthermore, the optimal rotation speed determined by the threshold effect is selected as the reaction condition for practical operation (blue line), and 650.8 g/L XA accumulated within 48 h, with a maximum productivity of 41.7 g/L/h and an average productivity of 13.6 g/L/h, reaching 95.8% of theoretical optimal results. Compared to the previously reported highest production level (586.3 g/L-120 h), the end titer of the product increased by 15.9%, and the catalytic efficiency increased by

about 14 times, achieving a breakthrough in XA production performance in hypertonic/hyperviscous reaction system, and strongly promoting the commercialization of XA biopreparation of XA in industry[43,44].

Conclusion

In response to the sharp contradiction between high titer products and large-scale oxygen demand in aerobic biocatalytic processes and the strong mass transfer resistance in hypertonic/hyperviscous systems, an effective process intensification strategy for whole-cell catalysis is established in this study. Through fluid flow characteristics analysis, CFD simulation, and oxygen transfer parameters exploration, multi-dimensional investigations are conducted on biochemical parameters such as viscosity, gas holdup, power number, and cell respiration rate. In addition, the theoretical threshold range of rotation speed is determined from the change in biochemical parameters, and the optimal catalytic model is established based on the threshold effect. Finally, in SOS-BR, an intensification strategy for producing XA with high concentration, efficiency, and quality is established by combining theory and practice, breaking through the viscosity limitation in a hypertonic/hyperviscous system. Overall, this intensification strategy provides valuable technical guidance and theoretical support to overcome the mass transfer bottleneck of high-viscosity reaction systems in an aerobic catalytic industry.

Table 1. The geometrical parameter of SOS-BR

Geometrical parameter	value	Geometrical parameter	value
Nominal volume	5.0 L	Stirring paddles number	2
Liquid volume	3.0 L	Stirring paddles thickness	2 mm
Bioreactor diameter	170 mm	Paddle blades length	21 mm
Bioreactor height	222 mm	Paddle blades width	16 mm
Broth height	130 mm	Paddle blades diameter	88 mm
Baffle number	4	Bottom propeller height	44 mm
Baffle length	157 mm	Upper propeller height	114 mm
Baffle width	10 mm	Sparger height	3 mm
Stirring shaft diameter	11 mm	Holes number in sparger	17
Sparger diameter	66 mm	Holes diameter	1 mm

Table 2. The calculation of rheological parameters of reaction systems with different xylose concentrations

Xylose (g/L)	Fitting line	R^2	n	k
50	y=-0.039x+0.197	0.979	0.961	1.26
100	y=-0.043x+0.333	0.972	0.957	1.45
200	y=-0.058x+0.754	0.979	0.942	2.24
300	y=-0.064x+1.070	0.979	0.936	3.08
400	y=-0.074x+1.518	0.990	0.926	4.87
500	y=-0.076x+1.874	0.985	0.924	6.96
600	y=-0.077x+2.274	0.990	0.923	10.40
700	y=-0.079x+2.500	0.987	0.921	13.05
800	y=-0.081x+2.917	0.991	0.919	19.84

Figure 1. Schematic diagram of oxygen transport from bubble to *G. oxydans*

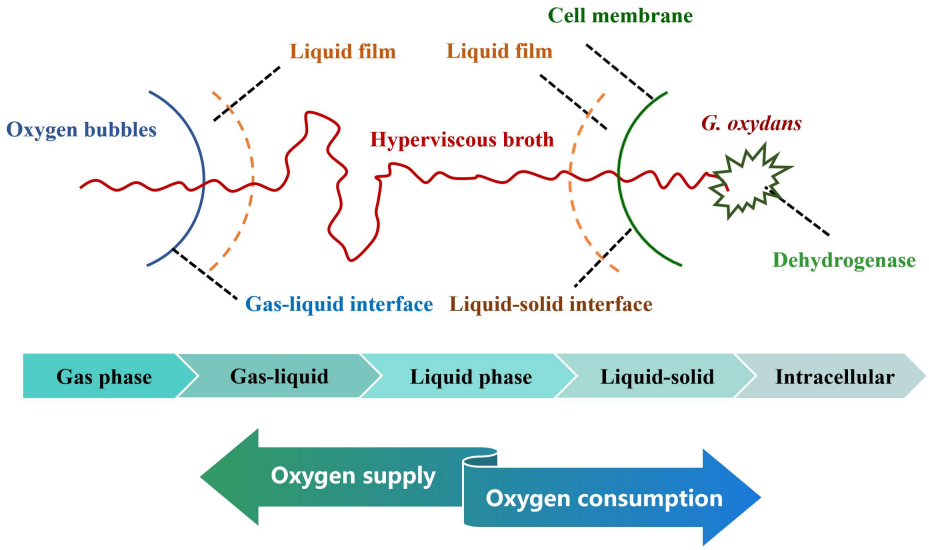

Figure 2. Schematic diagram of meshing division for bioreactor and internal stirring paddle simulated by CFD

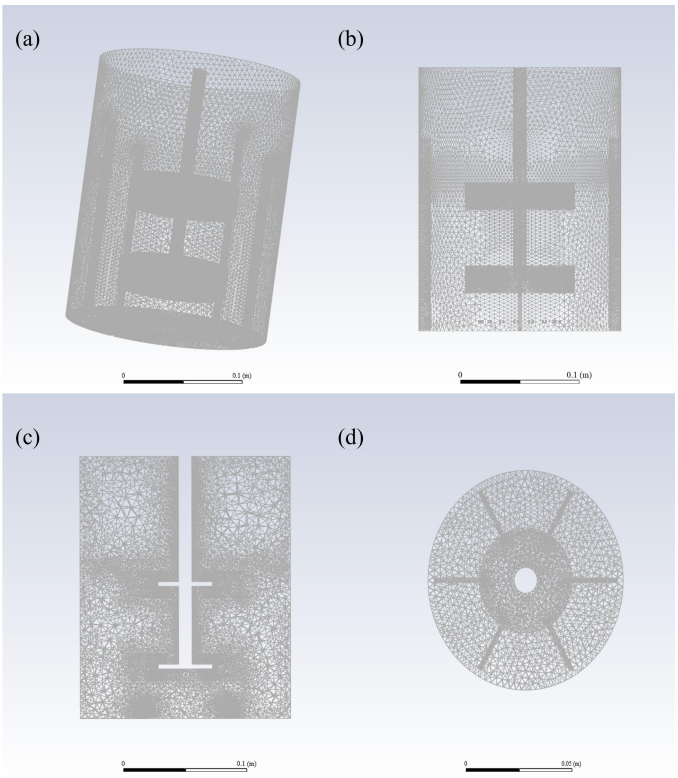

Figure 3. Dynamic method for measuring oxygen mass transfer parameters. The dynamic measurement process is divided into three stages. The first stage of stable gas supply; The second stage of gas supply cessation is used to calculate cell respiration rate q_{O_2}; The third stage of gas supply restoration is used to calculate the oxygen transfer coefficient $K_L\alpha$.

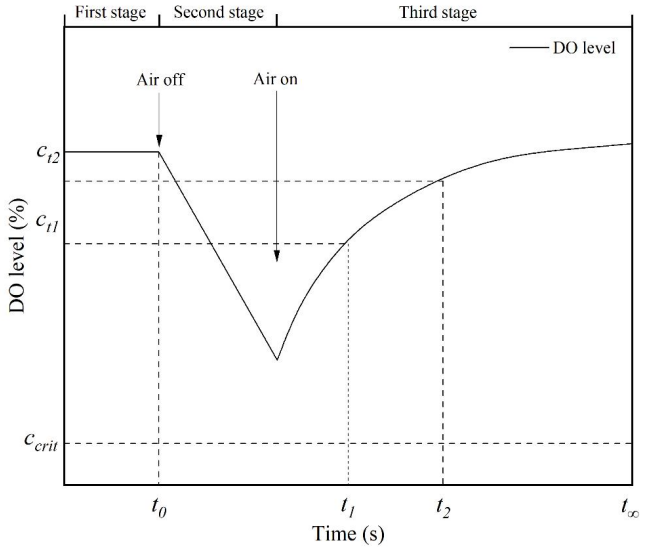

Figure 4. Relevant physical parameters of xylose and XA broth at different concentrations.

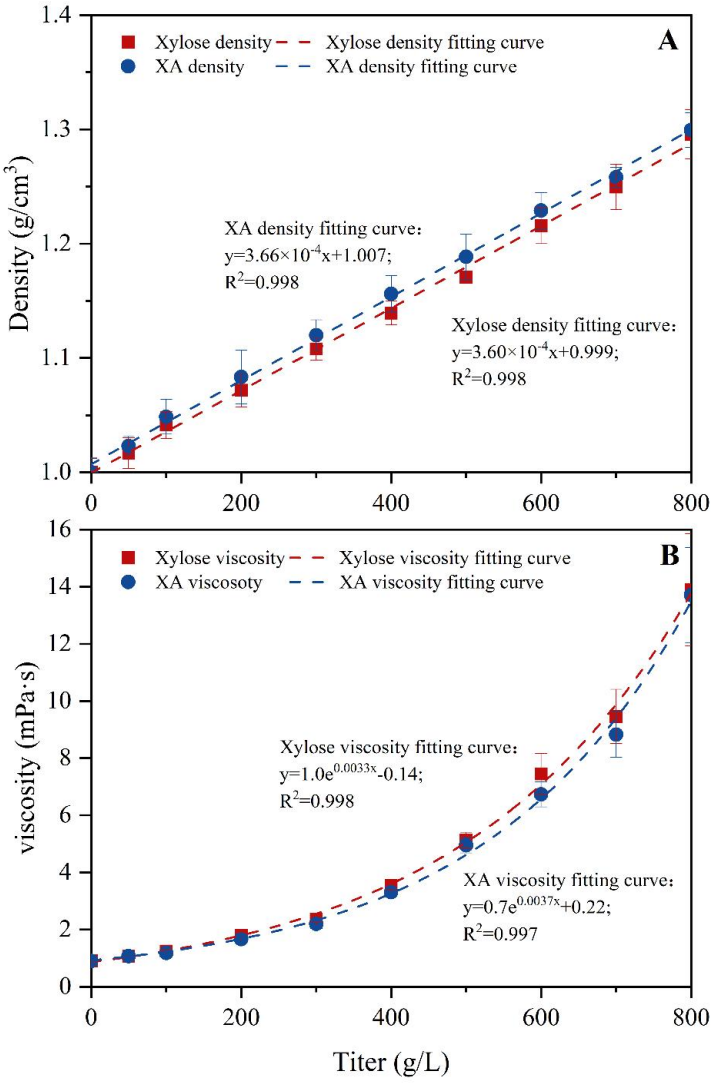

Figure 5. Viscosity variation trend of reaction systems with different xylose concentrations at different rotational speed.

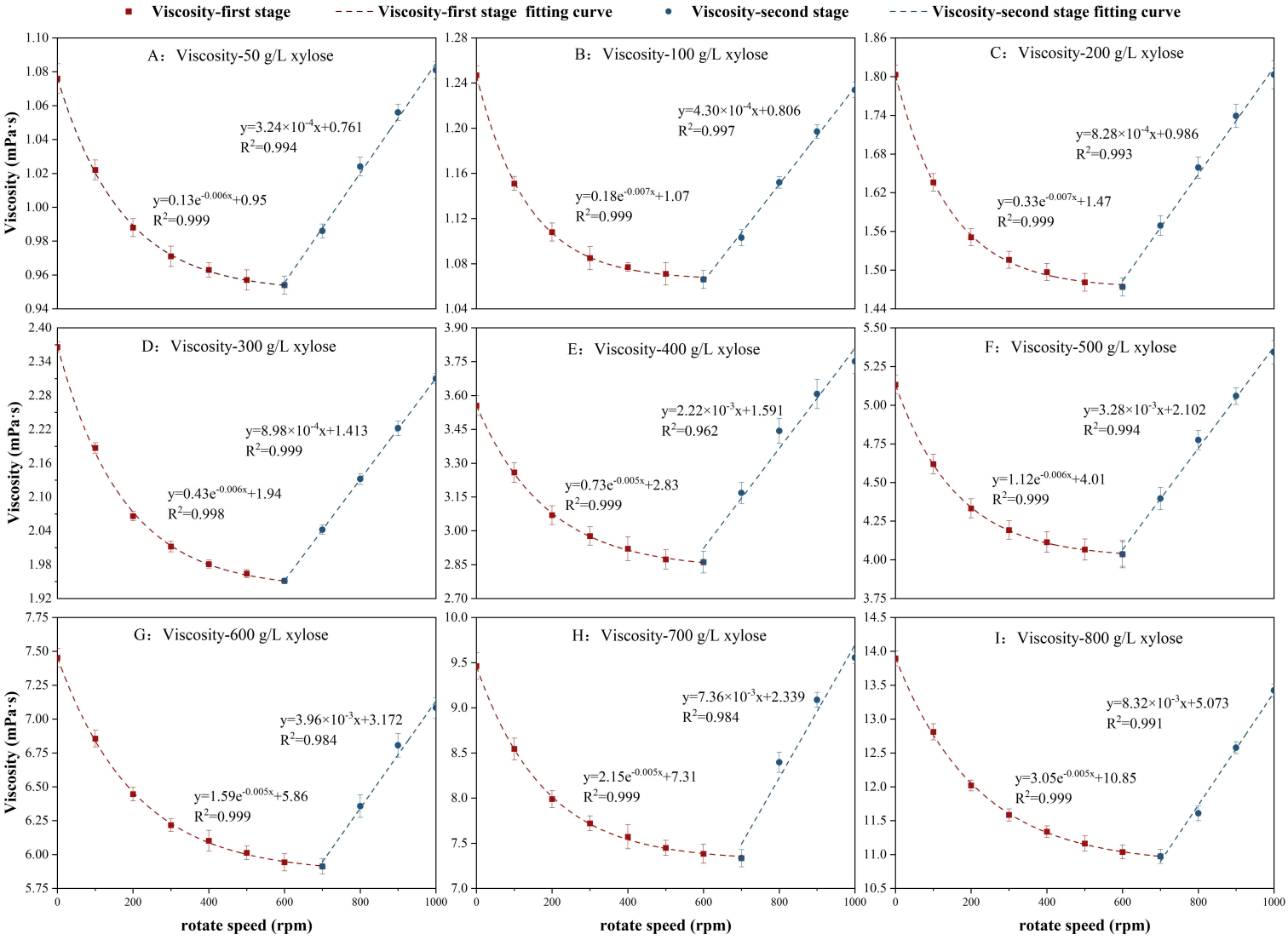

Figure 6. The fluid flow characteristics model between Inη and InN

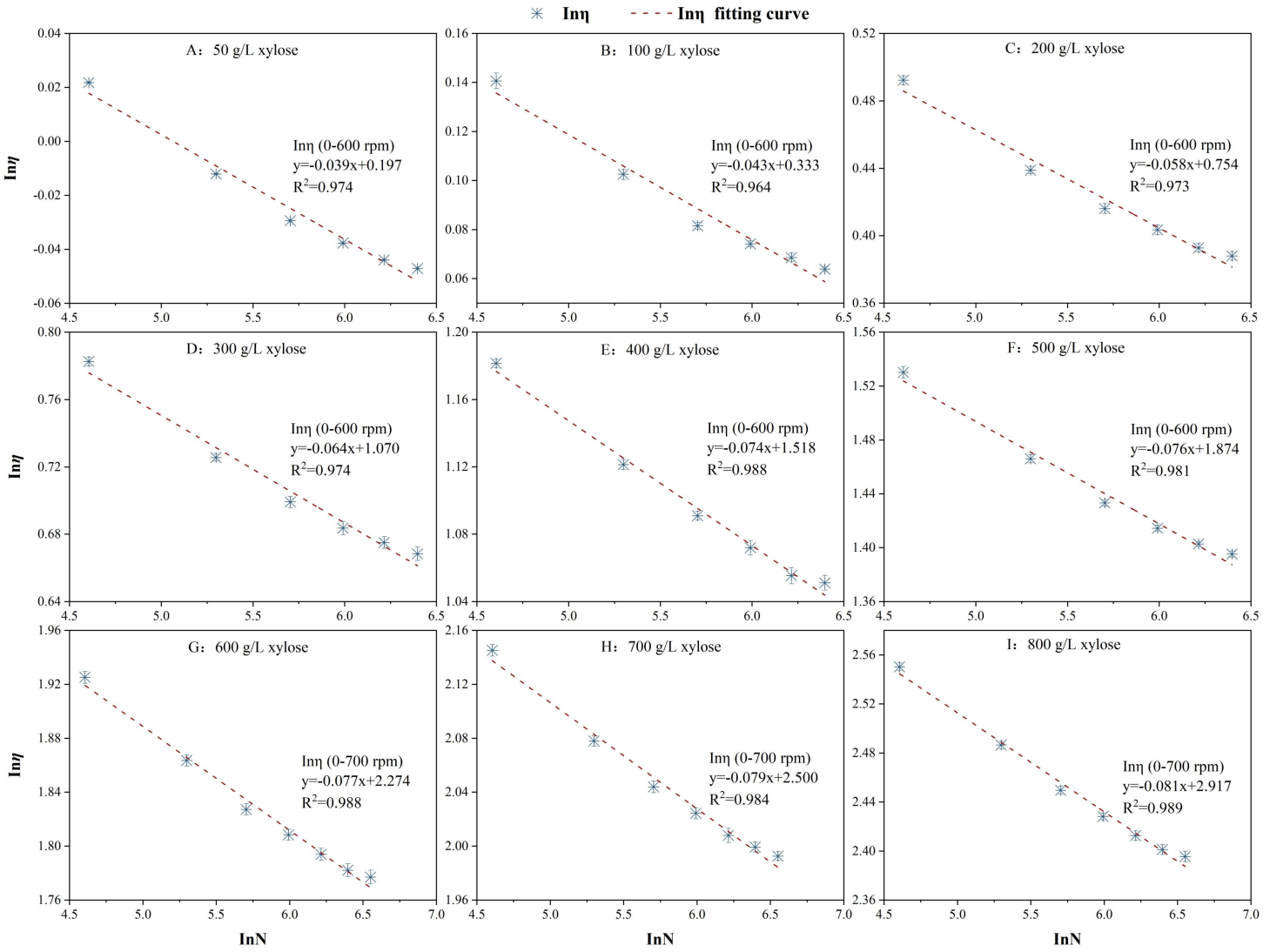

Figure 7. The cloud diagram of gas distribution at the middle cross-section of SOS-BR with different reaction condition. (1)-(5), (6)-(10), (11)-(15), (16)-(20) represents 100, 300, 500, 700 g/L xylose broth with 100/300/500/700/900 rpm.

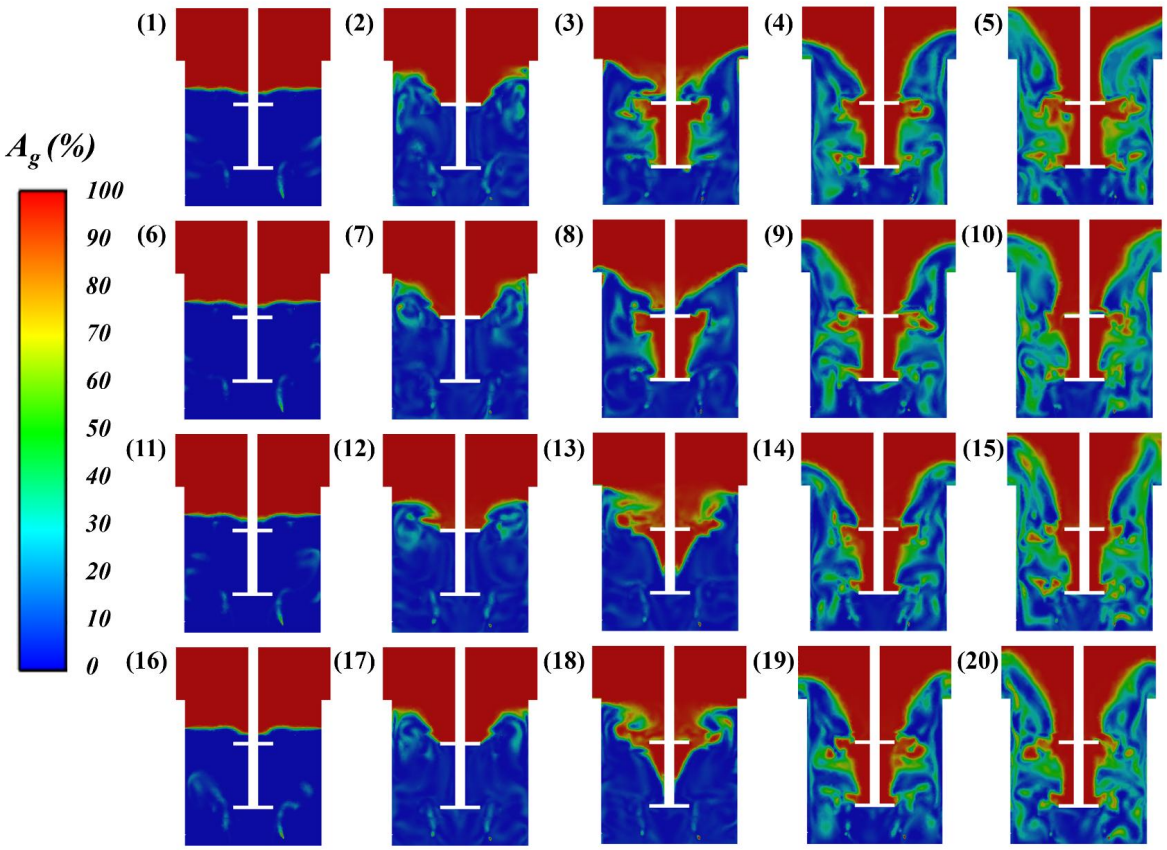

Figure 8. The threshold effect of gas holdup and power number in whole-cell catalysis by CFD simulation.

a. gas holdup α_g

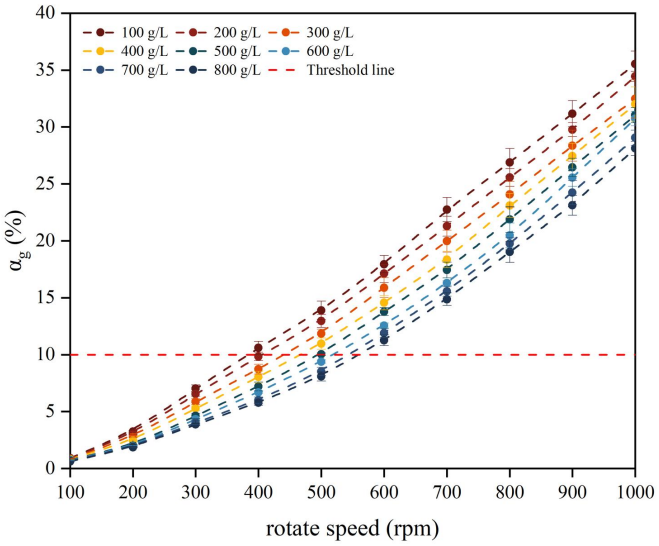

b. power number

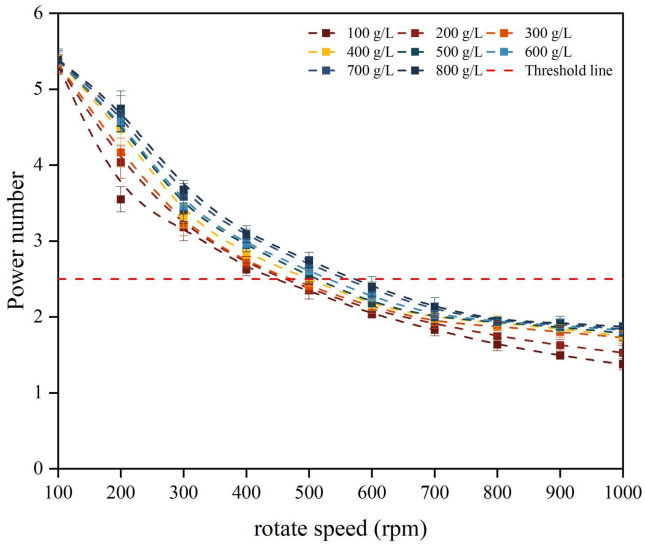

c. Threshold range

Xylose (g/L) / Threshold (rpm)	100	200	300	400	500	600	700	800
Gas holdup	>383	>404	>439	>465	>494	>518	>543	>559
Power number	>446	>460	>470	>499	>512	>529	>558	>572

Figure 9. Analysis of oxygen mass transfer mechanism and determination of threshold range.

a. dynamic determination process with 100-500 rpm

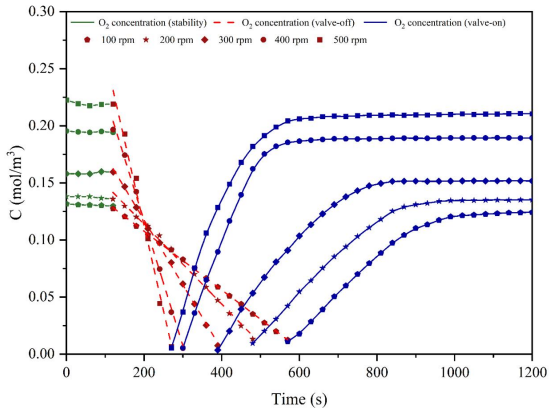

b. dynamic determination process with 600-1000 rpm

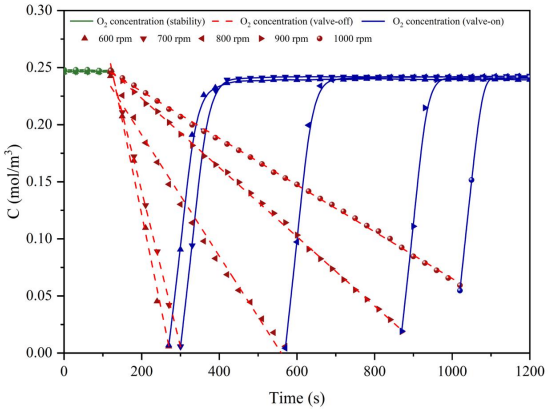

c. oxygen transfer parameters

Rotate speed (rpm)	Second stage fitting equation	q_{O_2} (mmol $O_2/g_x/h$)	Theoretical productivity (g/L/h)	$K_L a$ (h^{-1})
100	$y=-2.57\times10^{4}x+0.16$	0.46	1.39	9.89
200	$y=-3.49\times10^{-4}x+0.18$	0.63	1.89	13.3
300	$y=-5.66\times10^{-4}x+0.23$	1.02	3.06	17.79
400	$y=-1.09\times10^{-3}x+0.33$	1.96	5.89	27.77
500	$y=-1.49\times10^{-3}x+0.41$	2.68	8.05	41.05
600	$y=-1.65\times10^{-3}x+0.45$	2.97	8.91	65.12
700	$y=-1.36\times10^{-3}x+0.41$	2.45	7.34	103.87
800	$y=-5.31\times10^{-4}x+0.30$	0.96	2.87	143.39
900	$y=-3.03\times10^{-4}x+0.28$	0.55	1.64	181.18
1000	$y=-2.05\times10^{-4}x+0.27$	0.37	1.11	214.44

d. the theoretical XA productivity

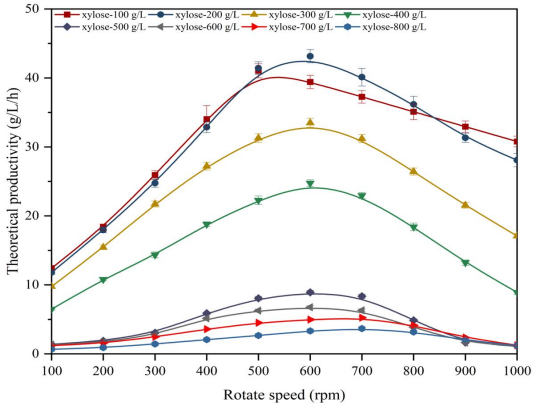

e. threshold range

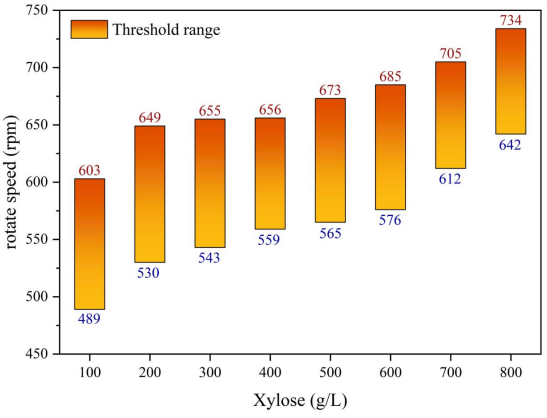

Figure 10. The whole-cell catalysis of xylose for XA biopreparation based on optimal threshold range.

a. summarize threshold range

Threshold (rpm) \ Xylose (g/L)	100	200	300	400	500	600	700	800
Viscosity	400-650	400-650	400-650	400-650	400-650	500-750	500-750	500-750
Gas holdup	>383	>404	>439	>465	>494	>518	>543	>559
Power number	>446	>460	>470	>499	>512	>529	>558	>572
Cell respiration rate	489-603	530-649	543-655	559-656	565-673	576-685	612-705	642-734
Summarize	489-603	530-649	543-650	559-650	565-650	576-685	612-705	642-734
Optimal	532	574	594	610	626	642	657	673

b. optimal model

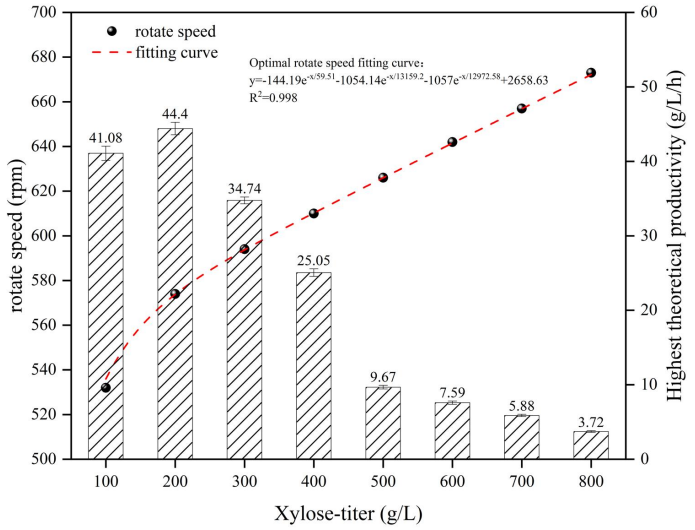

c. whole-cell catalysis

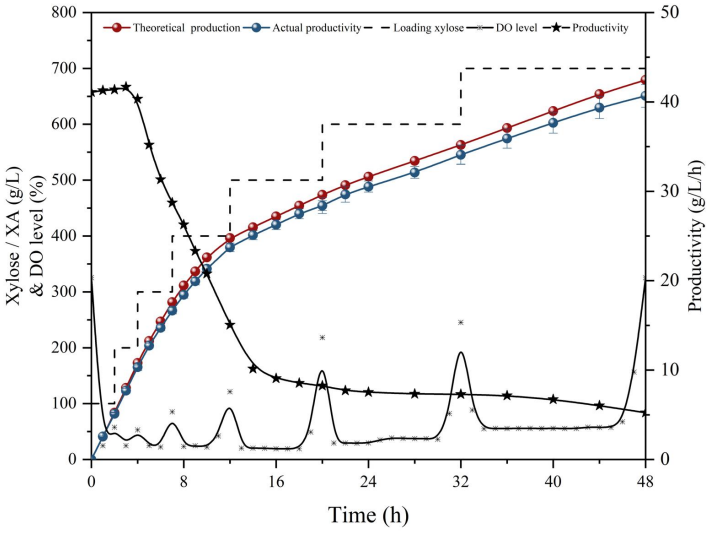

Data Availability and Reproducibility Statement

The authors declare that the data supporting the findings of this study are available in the article and Supplementary Material. Additional datasets related to this study are available from the corresponding authors on request.

The numerical data from Figures 1, 5, 6, 8–10 are tabulated in the Supplementary Material.

"Error bars (where shown) in Figures 4-8 and 9d and 10 show the spread of data observed in triplicate measurements, where independent samples were tested for each measurement. Experimental data shown without error bars in Figures 9a and 9b are from individual experimental measurements.

Acknowledgements

The research was supported by the National Natural Science Foundation of China (32211530071& 32171730), and Postdoctoral Fellowship Program of CPSF (GZB20230306). Also, the authors gratefully acknowledge financial support from 'Forestry Engineering First-class Discipline Construction Project of Nanjing Forestry University'.

Author information

Authors and Affiliations

College of Chemical Engineering, Nanjing Forestry University. No. 159 Longpan Road, Nanjing, CN

Xia Hua: hx0712@njfu.edu.cn

YaTing Hu: 1060597225@qq.com

Jian Han: 335933921@qq.com

HongSheng Zhang: 1005340025@qq.com

Xin Zhou: 839822915@qq.com

Yong Xu: xuyong@njfu.edu.cn

Ethics declarations

Competing interests

The authors declare no competing interests.

References:

1. Yu S, Zheng B, Chen Z & Huo Y. Metabolic engineering of Corynebacterium glutamicum for producing branched chain amino acids. *Microb. Cell. Fact.* **20**, 230 (2021).
2. Upton D J, McQueen-Mason S J & Wood A J. In silico evolution of Aspergillus niger organic acid production suggests strategies for switching acid output. *Biotechnol. Biofuels*. **13**, 27 (2020).
3. Matilla M A, Daddaoua A, Chini A, Morel B & Krell T. An auxin controls bacterial antibiotics production. *Nucleic. Acids. Res.* **46**, 11229-11238 (2018).
4. Garcia-Ochoa F, Castro E G & Santos V E. Oxygen transfer and uptake rates during xanthan gum production. *Enzyme. Microb. Technol.* **27**, 680-690 (2000).
5. Pedersen M B, Gaudu P, Lechardeur D, Petit M & Gruss A. Aerobic respiration metabolism in lactic acid bacteria and uses in biotechnology. *Annu. Rev. Food Sci. Technol.* **3**, 37-58 (2012).

6. Van Stroe-Biezen S A M, Janssen A P M & Janssen L J J. Solubility of oxygen in glucose solutions. *Anal. Chim. Acta*. **280**, 217-222 (1993).

7. Gonzalez J E, Long C P & Antoniewicz M R. Comprehensive analysis of glucose and xylose metabolism in Escherichia coli under aerobic and anaerobic conditions by 13C metabolic flux analysis. *Metab. Eng.* **39**, 9-18 (2017).

8. Wang J. et al. In situ photo-fenton-like tandem reaction for selective gluconic acid production from glucose photo-oxidation. *ACS Catal.* **13**, 2637-2646 (2023).

9. Alves L A, Almeida E Silva J B & Giulietti M. Solubility of d-Glucose in water and ethanol/water mixtures. *J. Chem. Eng. Data*. **52**, 2166-2170 (2007).

10. Li G. et al. Mass transfer, gas holdup, and kinetic models of batch and continuous fermentation in a novel rectangular dynamic membrane airlift bioreactor. *Engineering*. **13**, 153-163 (2022).

11. Garcia-Ochoa F & Gomez E. Bioreactor scale-up and oxygen transfer rate in microbial processes: An overview. *Biotechnol. Adv.* **27**, 153-176 (2009).

12. Skouteris G, Rodriguez-Garcia G, Reinecke S F & Hampel U. The use of pure oxygen for aeration in aerobic wastewater treatment: A review of its potential and limitations. *Bioresour. Technol.* **312**, 123595 (2020).

13. Tajsoleiman T, Mears L, Krühne U, Gernaey K V & Cornelissen S. An industrial perspective on scale-down challenges using miniaturized bioreactors. *Trends. Biotechnol.* **37**, 697-706 (2019).

14. Khakpour S. et al. Oxygen transport in hollow fibre membrane bioreactors for hepatic 3D cell culture: A parametric study. *J. Membr. Sci.* **544**, 312-322 (2017).

15. Bolic A. et al. A flexible well-mixed milliliter-scale reactor with high oxygen transfer rate for microbial cultivations. *Chem. Eng. J.* **303**, 655-666 (2016).

16. Hou W, Li L & Bao J. Oxygen Transfer in High Solids Loading and Highly Viscous Lignocellulose Hydrolysates. *Acs Sustain. Chem. Eng.* **5**, 11395-11402 (2017).

17. Wang Z. et al. Improved vitamin B12 production by step-wise reduction of oxygen uptake rate under dissolved oxygen limiting level during fermentation process. *Bioresour. Technol.* **101**, 2845-2852 (2010).

18. Whitman W G. The Two-Film Theory of Gas Absorption. *Int. J. Heat Mass Tran*. **5**, 429-433 (1924).

19. Maina S. et al. Volumetric oxygen transfer coefficient as fermentation control parameter to manipulate the production of either acetoin or D-2,3-butanediol using bakery waste. *Bioresour. Technol.* **335**, 125155 (2021).

20. Gong C, Xu X & Yang Q. Gas holdup at dynamic equilibrium region of a bubble column: Effect of bubble generator performance. *Chem. Eng. J.* **443**, 136382 (2022).

21. Crouvisier Urion K, Garcia R, Boussard A, Degrand L & Guiga W. Optimization of pure linoleic acid 13-HPX production by enzymatic reaction pathway: Unravelling oxygen transfer role. *Chem. Eng. J.* **430**, 132978 (2022).

22. Ripoll M, Lerma-Escalera J A, Morones-Ramírez J R, Rios-Solis L & Betancor L. New perspectives into Gluconobacter-catalysed biotransformations. *Biotechnol. Adv.* **65**, 108127 (2023).

23. Prust C. et al. Complete genome sequence of the acetic acid bacterium Gluconobacter oxydans. *Nat. Biotechnol.* **23**, 195-200 (2005).

24. De Muynck C. et al. The Genus Gluconobacter oxydans: comprehensive overview of biochemistry and biotechnological applications. *Crit. Rev. Biotechnol.* **27**, 147-171 (2007).

25. Schmitz A M. et al. Generation of a Gluconobacter oxydans knockout collection for improved extraction of rare earth elements. *Nat. Commun.* **12**, 6693 (2021).

26. Han J. et al. A cost-practical cell-recycling process for xylonic acid bioproduction from acidic lignocellulosic hydrolysate with whole-cell catalysis of Gluconobacter oxydans. *Bioresour. Technol.* **333**, 125157 (2021).

27. Hua X, Han J, Zhou X & Xu Y. Gas pressure intensifying oxygen transfer to significantly improving the bio-oxidation productivity of whole-cell catalysis. *Aiche J.* **69**, e18005 (2023).

28. Xu C. et al. Power consumption and oxygen transfer optimization for C5 sugar acid production in a gas-liquid stirred tank bioreactor using CFD-Taguchi method. *Renew. Energy*. **212**, 430-442 (2023).

29. Hua X, Du G, Han J & Xu Y. Bioprocess intensification for whole-cell catalysis of catabolized chemicals with 2,4-dinitrophenol uncoupling, *Acs Sustain. Chem. Eng.* ***8***, 15782-15790 (2020).

30. Hua X, Zhang C, Han J & Xu Y. A wholly biological method for galactaric acid production from pectin by the combination of enzymatic hydrolysis and resting-cell catalysis. *Green Chem.* **24**, 5197-5203 (2022).

31. Shu L. et al. Process optimization in a stirred tank bioreactor based on CFD-Taguchi method: A case study. *J. Clean. Prod.* **230**, 1074-1084 (2019).

32. Park S, Na J, Kim M & Lee J M. Multi-objective Bayesian optimization of chemical reactor design using computational fluid dynamics. *Comput. Chem. Eng.* **119**, 25-37 (2018).

33. Hua X, Zhou X, Du G & Xu Y. Resolving the formidable barrier of oxygen transferring rate (OTR) in ultrahigh-titer bioconversion/biocatalysis by a sealed-oxygen supply biotechnology (SOS). *Biotechnol. Biofuels*. **13**, 1 (2020).

34. Hua X, Han J, Liu X & Xu Y. Cascading and precise regulation of the selective bio-production of 2- or 5-ketogluconic acid from glucose with whole-cell catalysis technology. *Green Chem.* **25**, 2378-2386 (2023).

35. Bell E L. et al. Biocatalysis. *Nat. Rev. Method. Prime*. **1**, 46 (2021).

36. Sun T. et al. Structure, rheology, and antifreeze property of the exopolysaccharide from Naematelia aurantialba through basidiospore fermentation. *Food Hydrocoll.* **142**, 108848 (2023).

37. Batista R D. et al. Physicochemical, functional and rheological properties of fermented and non-fermented starch from canary seed (Phalaris canariensis). *Food Hydrocoll.* **99**, 105346 (2020).

38. Sánchez Pérez J A, Rodríguez Porcel E M, Casas López J L, Fernández Sevilla J M & Chisti Y. Shear rate in stirred tank and bubble column bioreactors. *Chem. Eng. J.* **124**, 1-5 (2006).

39. Garcia-Ochoa F, Gomez E & Santos V E. Fluid dynamic conditions and oxygen

availability effects on microbial cultures in STBR: An overview. *Biochem. Eng. J.* **164**, 107803 (2020).

40. Nadal-Rey G. et al. Understanding gradients in industrial bioreactors. *Biotechnol. Adv.* **46**, 107660 (2021).

41. Nauha E K, Kálal Z, Ali J M & Alopaeus V. Compartmental modeling of large stirred tank bioreactors with high gas volume fractions. *Chem. Eng. J.* **334**, 2319-2334 (2018).

42. Rivadeneyra-Romero G. et al. Intensification of power efficiency by grooves in flanged impellers. *Chem. Eng. J.* **470**, 144092 (2023).

43. Zhou X, Zhou X & Xu Y. Improvement of fermentation performance of Gluconobacter oxydans by combination of enhanced oxygen mass transfer in compressed-oxygen-supplied sealed system and cell-recycle technique. *Bioresour. Technol.* **244**, 1137-1141 (2017).

44. Zhou X, Lü S, Xu Y, Mo Y & Yu S. Improving the performance of cell biocatalysis and the productivity of xylonic acid using a compressed oxygen supply. *Biochem. Eng. J.* **93**, 196-199 (2015).